# Alternating substrate/ligand-metal coordination enables a low-energy pathway for C-O bond cleavage in the electrocatalytic reduction of carbon dioxide

Hemlata Agarwala,*[a,§] Xiaoyu Chen,[b,§] Julien R. Lyonnet,[a,‡] Ben A. Johnson,[a] Mårten Ahlquist*[b] and Sascha Ott*[a]

[a]*Department of Chemistry – Ångström Laboratories, Uppsala University, Box 523, 75120 Uppsala, Sweden.*

[b]*Department of Theoretical Chemistry and Biology, School of Engineering Sciences in Chemistry, Biotechnology and Health, KTH Royal Institute of Technology, 10691 Stockholm, Sweden.*

[‡]*Present address: Institute of Chemical Research of Catalonia (ICIQ), The Barcelona Institute of Science and Technology, 43007 Tarragona, Spain; ICREA, 08010 Barcelona, Spain.*

[§]*These authors have contributed equally.*

*Correspondence to: hemlata.agarwala@kemi.uu.se (ORCID: 0000-0001-7347-3093)

ahlqui@kth.se (ORCID: 0000-0002-1553-4027)

sascha.ott@kemi.uu.se (ORCID: 0000-0002-1691-729X)

ORCID identifiers of remaining authors: Xiaoyu Chen (0000-0002-7283-8676)

Ben A. Johnson (0000-0002-6570-6392)

*Supplementary Information (ESI) available*: Experimental and computational details, spectra, figures, tables.

## Abstract

Molecular electrocatalysts for $CO_2$-to-CO conversion often operate at large overpotentials, with the cleavage of a C-O bond in the [metal-$CO_2$]$^{n+}$ intermediate largely contributing to this unfavourable phenomenon. In natural CO dehydrogenase enzymes as well as synthetic systems, it has been shown that additional Lewis acids can aid in weakening the C-O bond by *O*-coordination. Illustrated with ruthenium-based $CO_2$ reduction electrocatalysts, [(*t*Bu$_3$tpy)(pp)Ru(CH$_3$CN)]$^{2+}$ (*t*Bu$_3$tpy = 4,4′,4″-tri-*tert*-butyl-2,2′:6′,2″-terpyridine; pp = bidentate polypyridine), we herein present computational and experimental evidence for a mechanistic route that involves one metal center that acts as both Lewis base and Lewis acid at different stages of the catalytic cycle. The nucleophilic character of the Ru center manifests itself in the initial attack at the $CO_2$ substrate to form [**Ru**-$CO_2$]$^0$, while its electrophilic character allows for the formation of a 5-membered metallacyclic intermediate, [**Ru**-$CO_2CO_2$]$^{0,c}$, by intramolecular cyclization of a linear [**Ru**-$CO_2CO_2$]$^0$ species that is formed from [**Ru**-$CO_2$]$^0$ and a second equivalent of $CO_2$. The pathway is enabled by the flexible ligation of polypyridine ligands that liberate coordination sites upon demand, and preferable coordination of carboxylate-$O^-$ to Ru over pyridine-*N*. The cyclic intermediate, [**Ru**-$CO_2CO_2$]$^{0,c}$, is crucial for energy-conserving turnover, as it allows for a third reduction at a more positive potential than that of the starting complex **Ru**$^{2+}$. The calculated activation barrier for C-O bond cleavage in [**Ru**-$CO_2CO_2$]$^{-1,c}$ is dramatically decreased to merely 8.5 kcal mol$^{-1}$ (pp = 6-methyl-2,2′-bipyridine) as compared to the 60 kcal mol$^{-1}$ required for C-O bond cleavage in the non-cyclic [**Ru**-$CO_2CO_2$]$^0$ adduct. The ruthenacyclic intermediates have been characterized experimentally by FTIR and $^{13}$C NMR spectroscopy and been corroborated by density functional theory (DFT) investigations. The present report is the first of its kind that experimentally observes metallacyclic intermediates in electrocatalytic $CO_2$ reduction, offering a new design feature that can be implemented consciously in future catalyst designs.

## Introduction

Electrochemical reduction of $CO_2$ can assist in mitigating atmospheric $CO_2$ levels and offer scalable means to store renewable electricity in energy dense compounds such as CO. Unfortunately, the electrochemical conversion of $CO_2$ to CO typically suffers from high overpotentials that impede efficient implementation.[1-3] In molecular transition metal-based catalysts, three key steps have been identified as potential kinetic bottlenecks: 1) $CO_2$ binding to the catalyst that is accompanied by bending of linear $CO_2$, 2) cleavage of a C-O bond in the [metal-$CO_2$]$^{n+}$ adduct and 3) CO dissociation from the catalyst. Of these three steps, the current report focuses mainly on C-O bond cleavage by molecular catalysts. Excessive electrochemical reduction steps have been shown to facilitate this process, but they typically occur at more negative standard potentials, thus leading to high overpotentials.[4-10] In nature, carbon monoxide dehydrogenase enzymes (CODH) can efficiently and reversibly convert CO to $CO_2$.[11] In the active site of CODH from the anaerobic bacterium *C. hydrogenoformans*, there is a [Ni-4Fe-5S] cluster, called the *C*-cluster, which consists of a [Ni-3Fe-4S] cubane linked to a unique Fe site through a sulfide.[12, 13] In this cluster, Ni is the redox active center to which $CO_2$ binds. In close proximity is a redox inactive Fe(III) Lewis acid that facilitates C-O cleavage by stabilizing the $OH^-$ group formed during the process.[13] Efforts to mimic this function in artificial systems include the simple addition of Brønsted acids to enhance catalytic activity.[4, 5, 7, 10, 14-36] Also, several metal complexes with intramolecular Brønsted acidic groups positioned close to the reactive center have been shown to facilitate C-O cleavage.[3, 10, 29, 35, 37-52]

Examples of catalytic rate enhancements for $CO_2$ electroreduction by Lewis acidic metal ions in molecular catalysts are comparatively rare.[32, 53-55] In some of these systems, cyclic intermediates that comprise the catalytic metal center, two molecules of $CO_2$ and an exogenous alkali or alkaline earth metal Lewis acid have been proposed[53-55] (Figs. 1a-1c); however, to the best of our knowledge, none was observed experimentally. It has been postulated that C-O cleavage from these cyclic intermediates is more facile compared to the systems without the additional Lewis acid.

Herein, we report a unique pathway for C-O bond cleavage in the overall reductive disproportionation of $CO_2$ to CO and $CO_3^{2-}$ that requires neither excessive catalyst reductions nor external Lewis acids. We present computational and experimental evidence for a mechanistic route that involves *one* metal center that acts as both Lewis base and Lewis acid at different stages of the catalytic cycle. The pathway is enabled by the flexible ligation of polypyridine ligands that can liberate coordination sites upon demand (Figs. 1(i) and 1(ii)).

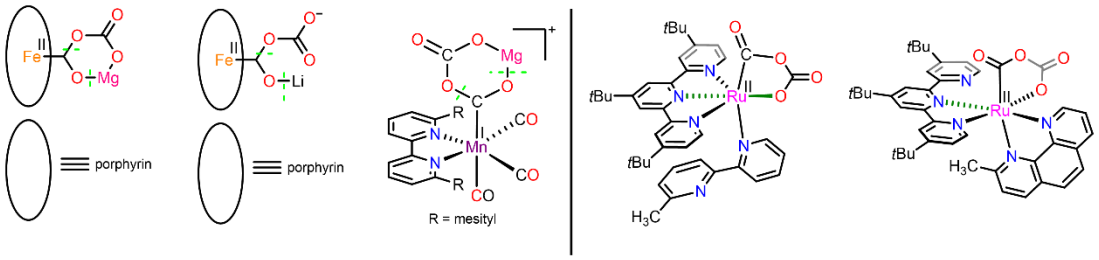


**Fig. 1** Representations of some transition metal-bound $CO_2$ adducts: (a-c) previously proposed, stabilized by Lewis acid (LA) cations like $Mg^{2+}$ and $Li^{+}$; (i and ii) investigated in the present work. The dashed green lines (----) indicate the scission of C-O and O-LA bonds in the subsequent step of the respective catalytic cycles.

## Results and discussion

The aforementioned mechanism is exemplified on two Ru-based catalysts, $[Ru(t\mathrm{Bu_3tpy})(CH_3bpy)(CH_3CN)]^{2+}$ ($\mathbf{1}^{2+}$)[56, 57] and $[Ru(t\mathrm{Bu_3tpy})(CH_3phen)(CH_3CN)]^{2+}$ ($\mathbf{2}^{2+}$) (Scheme 1; $t\mathrm{Bu_3tpy}$ = 4,4′,4″-tri-*tert*-butyl-2,2′:6′,2″-terpyridine; $CH_3bpy$ = 6-methyl-2,2′-bipyridine, $CH_3phen$ = 2-methyl-1,10-phenanthroline) that differ in the bidentate ligand motif.

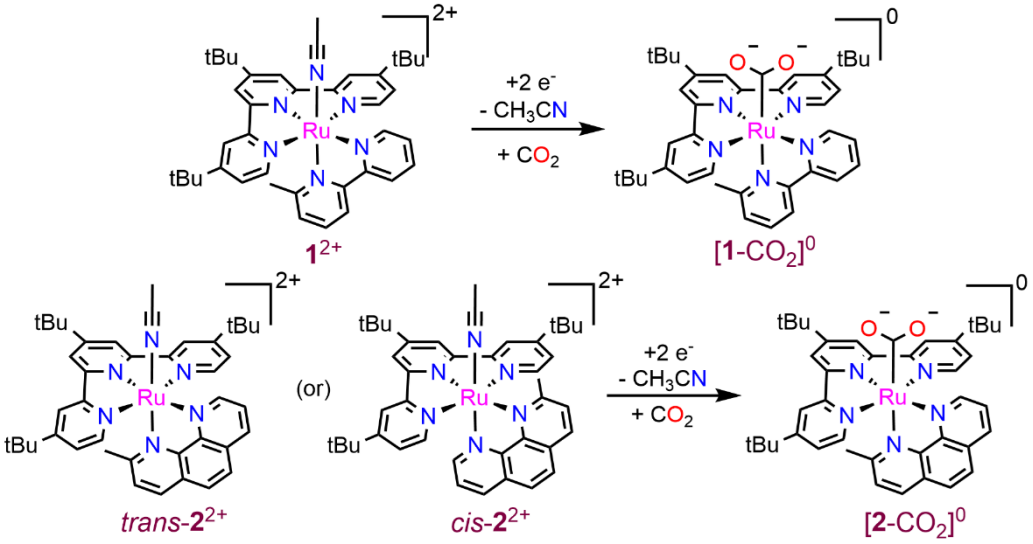


**Scheme 1.** Pictorial representation of complexes $\mathbf{1}^{2+}$ and $\mathbf{2}^{2+}$ (*cis* and *trans* isomers), and their two-electron reduced $CO_2$ adducts $[\mathbf{1}\text{-}CO_2]^0$ and $[\mathbf{2}\text{-}CO_2]^0$, respectively.

The bidentate phenanthroline in $\mathbf{2}^{2+}$ is a stronger coordinating ligand than 2,2′-bipyridine in $\mathbf{1}^{2+}$. The presence of the methyl group *ortho* to the nitrogen in the bidentate ligand is motivated by our previous finding that it labilizes the coordinated $CH_3CN$ upon one-electron reduction of the complex.[56]

Complexes $\mathbf{1}^{2+}$ and $\mathbf{2}^{2+}$ were prepared from $Ru^{III}(t\mathrm{Bu_3tpy})(Cl)_3$ and the respective bidentate ligand by slight modifications of published procedures[56] (see ESI for details). While $\mathbf{1}^{2+}$ is isolated solely in its *trans* form[56] (Scheme 1, top), the NMR spectrum of $\mathbf{2}^{2+}$ (Fig. S2) indicates

the presence of two coordination isomers (Fig. S2(a)) that differ in the position of the methyl group in the bidentate ligand with respect to the coordinated $CH_3CN$ (depicted as *cis*-$\mathbf{2}^{2+}$ and *trans*-$\mathbf{2}^{2+}$ in Scheme 1). The two forms are in dynamic equilibrium, as isolated *cis*-$\mathbf{2}^{2+}$ partially isomerizes to *trans*-$\mathbf{2}^{2+}$ when left in $CH_3CN$ for several days, as observed by its NMR spectrum (Figs. S2(b) and S2(d)).

As mentioned above, owing to the *ortho* methyl groups of the bidentate ligand, both complexes can liberate the $CH_3CN$ ligand upon one-electron reduction.[56] The coordinatively unsaturated intermediate acts as a Lewis base towards $CO_2$, ultimately leading to the two-electron reduced $CO_2$ adducts [**1**-$CO_2$]$^0$ and [**2**-$CO_2$]$^0$ (Scheme 1)[56] which are the starting points of the present study. In case of [**2**-$CO_2$]$^0$, DFT calculations indicate that both isomers of $\mathbf{2}^{2+}$ lead to the *trans*-[**2**-$CO_2$]$^0$ isomer shown in Scheme 1, as the nucleophilic attack of the reduced, pentacoordinate Ru center on $CO_2$ occurs from the sterically least occupied side of the complex (Scheme S1).

The cyclic voltammograms (CVs) of complexes $\mathbf{1}^{2+}$ and $\mathbf{2}^{2+}$ show electrochemically reversible one-electron reductions under argon at −1.76 V and −1.77 V *versus* $Fc^{+/0}$ respectively (Fig. 2, Table S1). Upon addition of $CO_2$ (0.28 M)[58], the first reductions become irreversible with noticeable enhancement in cathodic current, indicative of the electrochemical disproportionation of $CO_2$ to CO and $CO_3^{2-}$.

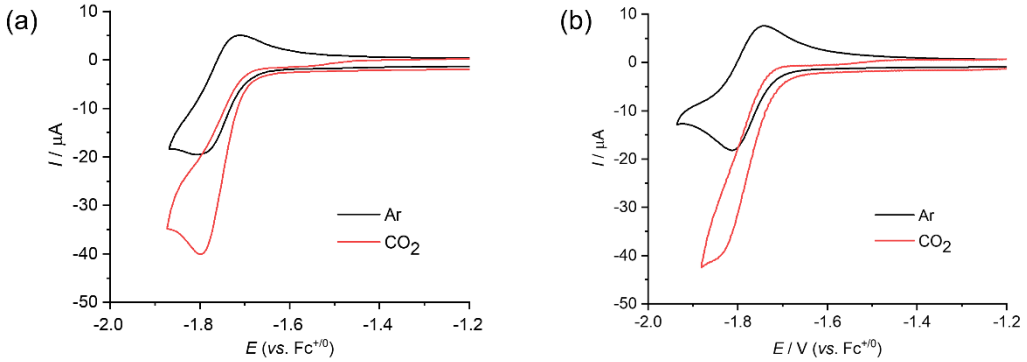


**Fig. 2** Cyclic voltammograms (shown is the first reduction) under Ar (black) and $CO_2$ (red; 0.28 M) of 1.0 mM solutions of (a) **1**$(PF_6)_2$ and (b) **2**$(PF_6)_2$. $\nu = 0.1$ V s$^{-1}$, $CH_3CN$/0.1 M $TBAPF_6$.

As discussed above, C-O bond cleavage is one of the kinetic bottlenecks in $CO_2$ reduction chemistry, and mechanistic details of this step have hitherto been elusive for [**1**-$CO_2$]$^0$ and [**2**-$CO_2$]$^0$. It is well documented for related systems that in the absence of any exogenous Lewis acids such as protons or metal salts, the oxygen of the metal-bound $CO_2$ is sufficiently nucleophilic to attack a second $CO_2$ molecule.[55-57, 59]

DFT calculations show that this is also the preferred pathway for [**1**-$CO_2$]$^0$ and [**2**-$CO_2$]$^0$, thereby producing [**1**-$CO_2CO_2$]$^0$ and [**2**-$CO_2CO_2$]$^0$, respectively (Figs. 3 and 4). The activation energy ($\Delta G^{\ddagger}$) for this step is calculated to be 15.4 kcal mol$^{-1}$ and 10.9 kcal mol$^{-1}$ for [**1**-$CO_2$]$^0$ and [**2**-$CO_2$]$^0$, respectively, with corresponding reaction free energies of 8.0 kcal mol$^{-1}$ and 4.1 kcal mol$^{-1}$.

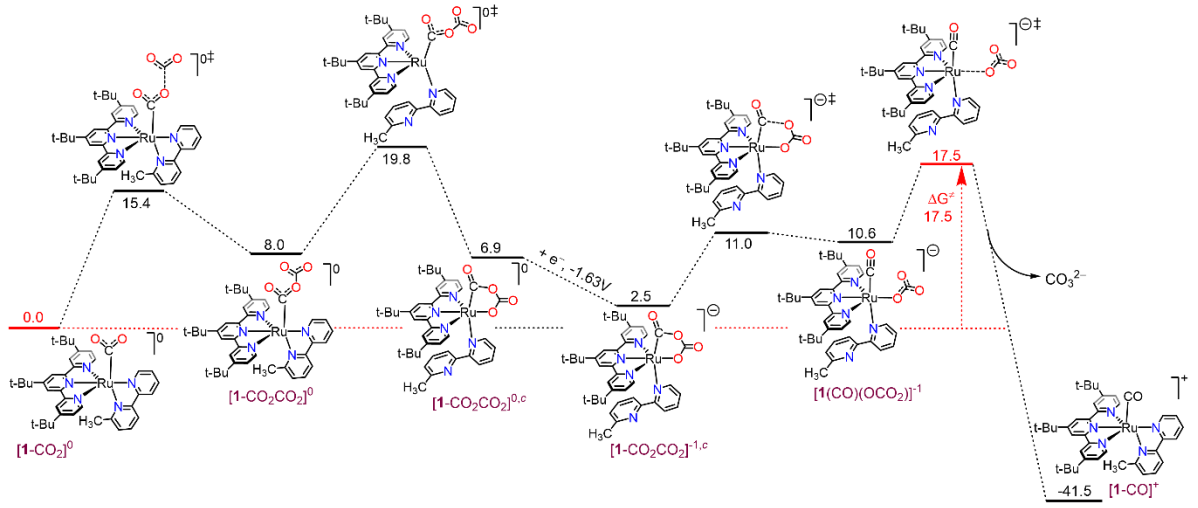


**Fig. 3** DFT calculated pathway from [**1**-$CO_2$]$^0$ to $CO_3^{2-}$ via the cyclic three-electron reduced intermediate [**1**-$COOCO_2$]$^{-1,c}$ at an applied potential of −1.82 V *versus* $Fc^{+/0}$ in $CH_3CN$.

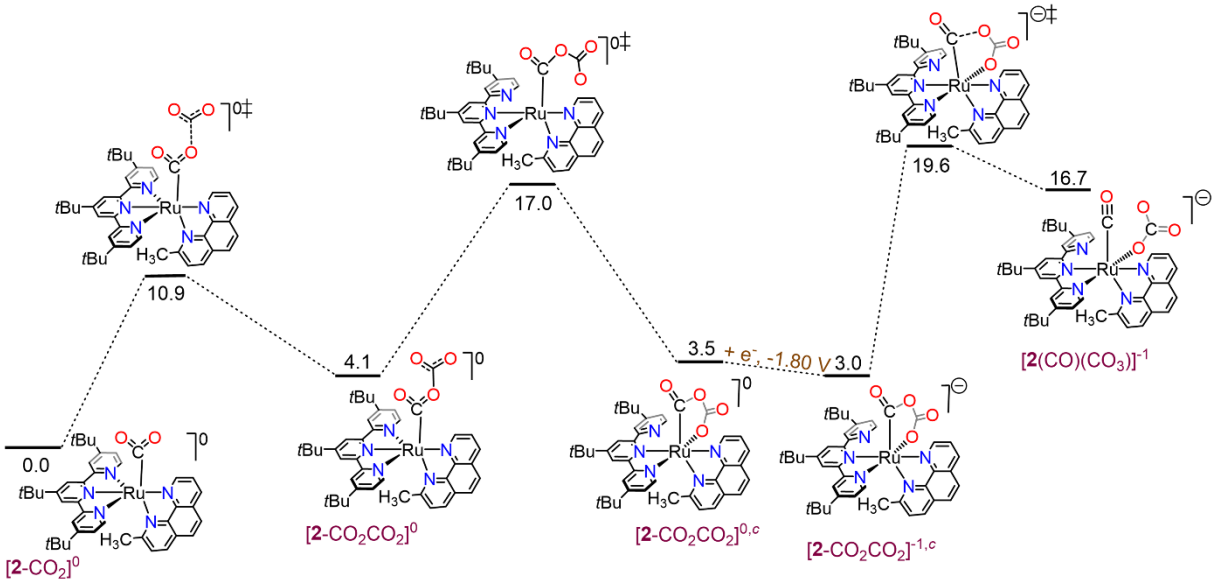


**Fig. 4** DFT calculated pathway to [**2**(CO)($CO_3$)]$^{-1}$ *via* the cyclic three-electron reduced intermediate [**2**-$CO_2CO_2$]$^{-1,c}$ at an applied potential of −1.82 V *versus* $Fc^{+/0}$ in $CH_3CN$.

While [**1**-$CO_2CO_2$]$^0$ is a plausible intermediate in the catalytic cycle, direct C-O bond cleavage to produce $CO_3^{2-}$ and the carbonyl complex (Scheme S2(a)) is not a viable option, as the calculated $\Delta G^{\ddagger}$ for this reaction is extremely high (60.5 kcal mol$^{-1}$). Moreover, electrochemical reduction of [**1**-$CO_2CO_2$]$^0$ to further weaken the aforementioned C-O bond is also unlikely because the calculated standard potential at −2.06 V (*versus* $Fc^{+/0}$) is significantly more negative than the applied potential (−1.82 V *versus* $Fc^{+/0}$)[56]. Alternatively, the negatively charged terminal oxygen in [**1**-$CO_2CO_2$]$^0$ could potentially attack the Ru center of a second 5-coordinate intermediate that is obtained by dissociation of $CH_3CN$ from one-electron reduced **1**$^+$.[56] Such an intermolecular attack would form a bimetallic intermediate with a -C(O)O-C(O)O- bridge (Scheme S2(b)), similar to the one proposed for $Re^I$(bpy)$(CO)_3$X catalysts.[60-62] However, this

scenario is unlikely as well given that the catalytic current shows a first order dependence on catalyst concentration in the range 0.05 mM to 1.0 mM as reported previously.[56]

In the absence of any other established literature pathway, we hypothesized whether a structural reorganization of the complex, either to facilitate C-O bond cleavage or to drive a third reduction at a more positive potential, could provide an energetically plausible pathway. A closer inspection of [**1**-$CO_2CO_2$]$^0$ shows that both -$CO_2CO_2$ and -$CH_3$bpy are bidentate ligands. Hence, the possibility of a ligand exchange between the equatorial pyridine of $CH_3$bpy and the terminal oxygen of -$CO_2CO_2$ to form [**1**-$CO_2CO_2$]$^{0,c}$ (Fig. 3) was explored. The reaction was found to have a $\Delta G^{\ddagger}$ of 11.8 kcal mol$^{-1}$, with [**1**-$CO_2CO_2$]$^{0,c}$ being more stable than [**1**-$CO_2CO_2$]$^0$ by 1.1 kcal mol$^{-1}$ (Fig. 3). The C-O bond that needs to be cleaved is elongated from 1.36 Å (in [**1**-$CO_2CO_2$]$^0$) to 1.42 Å (in [**1**-$CO_2CO_2$]$^{0,c}$), indicating enhanced single bond character.

Cyclic 5-membered metallacycles of this kind are not entirely unprecedented and have been reported in the reaction of low-valent metal species with $CO_2$, albeit in a *stoichiometric* fashion.[63-69] In context of catalytic $CO_2$ conversion, a related Co-based metallacycle was recently proposed by Lloret-Fillol and co-workers, however without any experimental evidence.[6] Partial de-coordination of polydentate polypyridyl ligands from metal centers upon reduction have also been postulated earlier by some groups.[70-72] However, the synergistic occurrence of these two processes in a single catalytic framework is, to the best of our knowledge, unprecedented.

Another interesting aspect of the cyclic intermediate [**1**-$CO_2CO_2$]$^{0,c}$ is that the intramolecular Lewis acid stabilization of the negative charge at the terminal *O* by the Ru center facilitates another reduction step from [**1**-$CO_2CO_2$]$^{0,c}$ to [**1**-$CO_2CO_2$]$^{-1,c}$. The potential for this reduction was calculated to be −1.63 V (*versus* $Fc^{+/0}$ in $CH_3CN$), thus more positive than the calculated standard potential of the [**1**-$CO_2CO_2$]$^{-1}$/[**1**-$CO_2CO_2$]$^0$ couple by 430 mV, and, more importantly, also more positive than the experimental applied potential of −1.82 V[56] (Fig. 3). The reason for this marked difference in reduction potential was found in the solvation free energies of the involved species. The linear isomer [**1**-$CO_2CO_2$]$^0$ is more polar compared to the cyclic one (Fig. 5), due to the negative charge on the terminal $CO_2$ in the former not being neutralized by the cationic Ru center, making it zwitterionic in nature. This leads to a significantly more negative solvation free energy of the linear conformer than that of the cyclic one (−58.3 for linear *versus* −37.4 kcal mol$^{-1}$ for cyclic; Table S2).

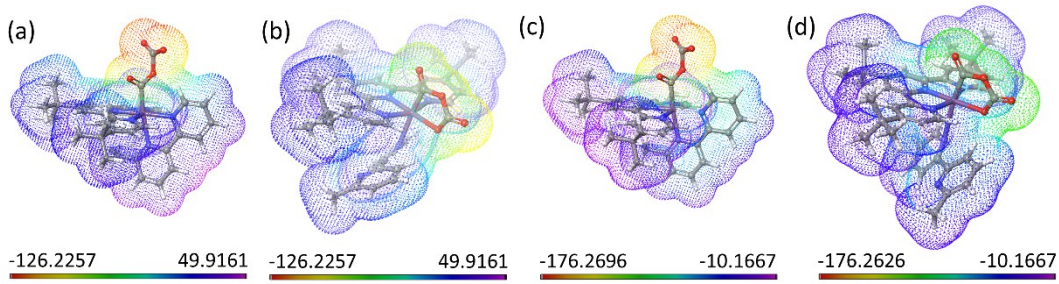


**Fig. 5** Plots of electrostatic potentials mapped onto electron density for (a) [**1**-$CO_2CO_2$]$^0$, (b) [**1**-$CO_2CO_2$]$^{0,c}$, (c) [**1**-$CO_2CO_2$]$^{-1}$ and (d) [**1**-$CO_2CO_2$]$^{-1,c}$. The values on the colour bars correspond to the range of electrostatic potentials (in kcal mol$^{-1}$); iso-value for electron density = 0.001 e Bohr$^{-3}$.

The reduction to the anionic intermediate increases the electron density on the Ru-polypyridyl fragment of the linear conformer, hence decreasing its overall zwitterionic character. This results in similar free energies of solvation for the two isomers; −82.5 *versus* −72.6 kcal mol$^{-1}$ for [**1**-$CO_2CO_2$]$^{-1}$ (linear) and [**1**-$CO_2CO_2$]$^{-1,c}$ (cyclic), respectively. Consequently, the difference in solvation free energy between the neutral and mono-anionic intermediates of the two isomers (Table S3) is −24.2 kcal mol$^{-1}$ and −35.2 kcal mol$^{-1}$ for the linear and the cyclic system, respectively, explaining the difference of 430 mV in their reduction potentials (−24.2 − (−35.2) = 11.0 kcal mol$^{-1}$ = 477 mV).

The structure of [**1**-$CO_2CO_2$]$^{-1,c}$ is similar to that of [**1**-$CO_2CO_2$]$^{0,c}$, with a relatively long C-O bond that is to be cleaved. The formation of the metallacycle also induces some strain, that further weakens the C-O bond, as evidenced by the small O-Ru-C angle of 79.7° in [**1**-$CO_2CO_2$]$^{-1,c}$. The transition state for C-O cleavage was located just 8.5 kcal mol$^{-1}$ above [**1**-$CO_2CO_2$]$^{-1,c}$, resulting in [**1**(CO)($OCO_2$)]$^{-1}$ at 10.6 kcal mol$^{-1}$ relative to [**1**-$CO_2$]$^0$. Dissociation of carbonate then proceeds with an activation energy at 17.5 kcal mol$^{-1}$ relative to [**1**-$CO_2$]$^0$, accompanied by restoration of the bidentate coordination mode of $CH_3$bpy to Ru (Fig. 3).

The highest activation energy barriers in Fig. 3 are for the formation of [**1**-$CO_2CO_2$]$^{0,c}$ at 19.8 kcal mol$^{-1}$ and the release of carbonate at a similar free energy of 17.5 kcal mol$^{-1}$. The barriers agree well with the experimental turnover frequency (TOF)[56] of 1.8 s$^{-1}$ which corresponds to an activation free energy of 17.2 kcal mol$^{-1}$ (see ESI for details).

Having identified the flexible coordination of the bidentate ligand and the subsequent formation of the [**1**-$CO_2CO_2$]$^{-1,c}$ metallacycle as crucial features for efficient C-O bond cleavage, focus was directed towards the phenanthroline analogue [2-$CO_2$]$^0$. As expected from the strong coordinating ability of the 2-Mephen ligand to the metal center, calculations show that partial de-coordination of the phenanthroline ligand is not feasible. However, the system has the possibility to find another pathway for the formation of a related cyclic intermediate, [**2**-$CO_2CO_2$]$^{0,c}$. This can be achieved by liberation of one of the pyridine units of the *t*$Bu_3$tpy ligand in [**2**-$CO_2CO_2$]$^0$ instead (Fig. 4). In analogy to the situation in [**1**-$CO_2CO_2$]$^{0,c}$, the formation of the cyclic intermediate [**2**-$CO_2CO_2$]$^{0,c}$ allows access to a further reduction at a potential (Fig. 4) that is less negative than that of the first reduction. The result is the three-electron reduced, cyclic adduct [**2**-$CO_2CO_2$]$^{-1,c}$ which is found as the lowest energy intermediate in the catalytic cycle (Fig. 4), just before C-O bond cleavage.

The relatively high computed stabilities of the cyclic intermediate [**1**-$CO_2CO_2$]$^{-1,c}$ and even more so [**2**-$CO_2CO_2$]$^{-1,c}$ indicate that their spectroscopic observation during electrocatalytic $CO_2$ reduction might be feasible. Experimentally, the relevant region in the infra-red (IR) spectra is convoluted by the evolution of three major bands at 1684 cm$^{-1}$, 1645 cm$^{-1}$ and 1304 cm$^{-1}$ that arise from the $CO_3^{2-}$ reductive disproportionation product (Fig. 6a).[56, 73] Nevertheless, the evolution of a weak shoulder at 1740 cm$^{-1}$ along with some unresolvable structured transitions near 1230 cm$^{-1}$ can be observed in the IR spectrum during the controlled potential electrolysis (CPE) of a 1.0 mM solution of $\mathbf{1}^{2+}$ in anhydrous $CH_3CN$ under $CO_2$ (0.28 M) (Fig. 6a).[56] DFT calculations show that these two absorptions most likely arise from a symmetric and an asymmetric C=O stretching vibration that are however ambiguous to assign to one particular species.[74] Both [**1**-$CO_2$]$^0$ (calc. at 1730 cm$^{-1}$ and 1235 cm$^{-1}$; Fig. S5(a)) and [**1**-$CO_2CO_2$]$^{-1,c}$

(calc. at 1759 $cm^{-1}$ and 1265 $cm^{-1}$; Fig. S5(b)) exhibit calculated IR vibrations that match the experimentally observed ones.

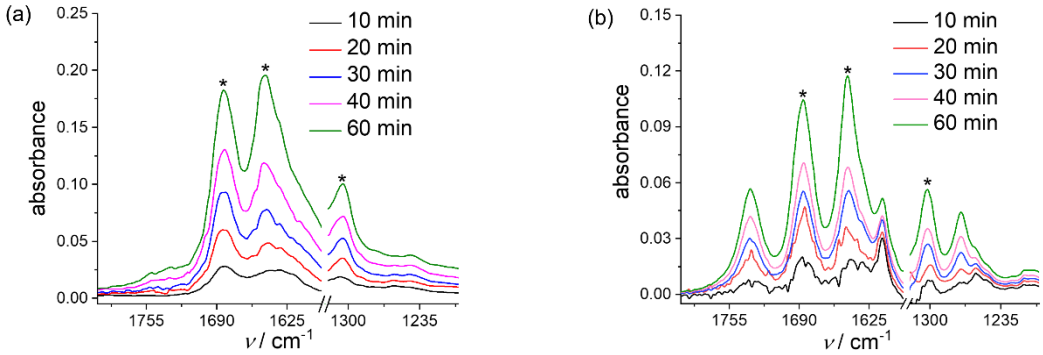


**Fig. 6** Fourier transformed infra-red (FT-IR) absorbance spectra of aliquots taken during controlled potential electrolysis of $CO_2$ saturated (0.28 M) solutions of (a) **1**$(PF_6)_2$ (1.0 mM) and (b) **2**$(PF_6)_2$ (1.0 mM), in anhydrous $CH_3CN$/0.1 M $TBAPF_6$ at an applied potential of −1.82 V (*versus* $Fc^{+/0}$). The peaks marked with * arise from the $CO_3^{2-}$.

IR spectra recorded during the CPE of $\mathbf{2}^{2+}$ at −1.82 V (*versus* $Fc^{+/0}$) under $CO_2$ (0.28 M) display the evolution of clearly visible bands at 1735, 1612 and 1272 $cm^{-1}$ along with those of the $CO_3^{2-}$ byproduct (Fig. 6b). The 1735 $cm^{-1}$ band can be explained by a C=O stretching vibration in either [**2**-$CO_2$]$^0$ or [**2**-$CO_2CO_2$]$^{0,c}$; (calc: 1729 $cm^{-1}$ and 1760 $cm^{-1}$, respectively; Fig. S6(a) and S6(c)), while no absorption is expected for [**2**-$CO_2CO_2$]$^{-1,c}$ in this range. The experimental IR absorption at 1272 $cm^{-1}$ corresponds very well to computed C-O stretches at 1253 $cm^{-1}$ and 1291 $cm^{-1}$ for [**2**-$CO_2CO_2$]$^{0,c}$ and [**2**-$CO_2CO_2$]$^{-1,c}$, respectively (Fig. S6(c) and S6(d)[75]), while the experimentally obtained peak at 1612 $cm^{-1}$ is only found in the calculated IR spectrum of [**2**-$CO_2CO_2$]$^{-1,c}$ at 1614 $cm^{-1}$ (Fig. 6b and S6(d)).

This unique absorption allows for the identification of [**2**-$CO_2CO_2$]$^{-1,c}$ as one of the intermediates accumulated during CPE. Altogether, the IR monitoring indicates the presence of [**2**-$CO_2$]$^0$, [**2**-$CO_2CO_2$]$^{0,c}$ and [**2**-$CO_2CO_2$]$^{-1,c}$ being built up during CPE, consistent with the small calculated energy differences between these intermediates (3.5 kcal $mol^{-1}$ between [**2**-$CO_2$]$^0$ and [**2**-$CO_2CO_2$]$^{0,c}$; 3.0 kcal $mol^{-1}$ between [**2**-$CO_2$]$^0$ and [**2**-$CO_2CO_2$]$^{-1,c}$; Fig. 4). Linear [**2**-$CO_2CO_2$]$^0$ is not present in detectable amounts, as its diagnostic calculated IR absorption at 1869 $cm^{-1}$ is absent from the experimental CPE monitoring (Fig. S7).

Conducting CPE of $\mathbf{2}^{2+}$ under identical conditions, but with $^{13}CO_2$ gives rise to FT-IR spectra that are qualitatively similar to the ones under $^{12}CO_2$, with the expected shifts due to the isotope labelling. The C=O and C-O stretching vibrations shift by 40-50 and 15-20 $cm^{-1}$ to lower wavenumbers,[74] respectively, when going from $^{12}CO_2$ to $^{13}CO_2$,[55, 62] confirming that these IR bands arise from $CO_2$ (Fig. S8). The calculated IR bands of [**2**-$^{13}CO_2{}^{13}CO_2$]$^{-1,c}$ agree well with the experimentally observed ones from CPE ($\nu$ ($cm^{-1}$): experimental (calc.): 1642 (1648), 1564 (1575) and 1279 (1265) $cm^{-1}$, Fig. S9).

The IR-spectroscopic observation of [**2**-$CO_2CO_2$]$^{-1,c}$ is consistent with a lower rate of C-O bond dissociation compared to that in [**1**-$CO_2CO_2$]$^{-1,c}$ as evidenced by a higher DFT calculated activation free energy (16.6 kcal $mol^{-1}$ for [**2**-$CO_2CO_2$]$^{-1,c}$ *versus* 8.5 kcal $mol^{-1}$ for [**1**-$CO_2CO_2$]$^{-1,c}$; Figs. 3 and 4). The IR signature of [**2**-$CO_2CO_2$]$^{-1,c}$ is very similar to that of the

reported complex $Ir(PMe_3)_3(Cl)(COOCOO)$ with a similar metallacycle consisting of two $CO_2$ molecules in a "head-to-tail" arrangement.[63] The latter was made by the stoichiometric reaction of a low-valent metal precursor and $CO_2$, and exhibits IR bands at 1725, 1680, 1648 (sh), 1605, and 1290 $cm^{-1}$.[63]

Further experimental support for the presence of cyclic intermediates during the catalytic cycle of $\mathbf{2}^{2+}$ was sought from $^{13}C$ NMR analysis after 1h CPE of an $CH_3CN$ solution under an atmosphere of isotopically labeled $^{13}CO_2$ (see ESI). Such experiments that involve the trapping of reaction intermediates *ex situ* are technically not trivial and, thus, the experiments were repeated multiple times. While the obtained individual $^{13}C$ NMR spectra showed qualitative differences, their collective interpretation gave a glimpse of the species involved (Fig. S10). First, the DEPT (Distortionless Enhancement by Polarization Transfer) $^{13}C$ NMR spectra of the samples showed no signals (Fig. S11), in the region where Ru-bound carboxylato intermediates derived from $^{13}CO_2$ would be expected.[65, 66, 76] The absence of such signals in the DEPT $^{13}C$ NMR spectra ascertain that all resonances observed in ordinary $^{13}C$ NMR spectra in this region arise from quaternary carbons. In all experiments, the $CO_3^{2-}$ byproduct features as a broad resonance at about 160.0 ppm (Fig. S10; $\delta$ = 160.9 ppm for tetraethylammonium bicarbonate in $CD_3CN$, Fig. S12), possibly as an *O*-bound **Ru**-carbonato species, like $[Ru(t\mathrm{Bu}_3\mathrm{tpy})(CH_3\mathrm{phen})(CO_3)]^+$, in analogy to the $^{13}C$ NMR chemical shift of previously reported $[Ru(CNC)(bpy)(CO_3)]^+$ (160.1 ppm in $CD_3CN$).[76] Dissolved $^{13}CO_2$ is observed at 125.8 ppm. Consistently observed in all experiments is a single resonance at ~164.3 ppm, albeit in varying intensity relative to the other signals (Fig. S10). It is thus safe to assume that this signal arises from a species that contains only one $CO_2$-derived ligand, which suggests an assignment to $[\mathbf{2}\text{-}CO_2]^0$. Other signals that are observed in the $^{13}C$ NMR spectra emerge in pairs of two, with one such set at ~157.5 ppm and ~165.0 ppm being present in all $^{13}C$ NMR experiments. Another pair of signals at 167.1 ppm and 169.1 ppm is only observed in some of the experiments. Considering the appearance of these signals in pairs, they are likely to arise from species that contain a $C_2O_4$–type ligand.

It is important to realize that species observed in the $^{13}C$ NMR experiments may not be the same as those detected by FT-IR spectroscopy, as, for example, reduced $[\mathbf{2}\text{-}CO_2CO_2]^{-1,c}$ will be oxidized to $[\mathbf{2}\text{-}CO_2CO_2]^{0,c}$ by trace amounts of oxygen introduced during NMR sample preparation. Given this re-oxidation to $[\mathbf{2}\text{-}CO_2CO_2]^{0,c}$, also $[\mathbf{2}\text{-}CO_2CO_2]^0$ can be expected in the NMR experiments, as the two species are basically iso-energetic (Fig. 4). With this reasoning, the two pairs of signals are tentatively assigned to cyclic $[\mathbf{2}\text{-}CO_2CO_2]^{0,c}$ and linear $[\mathbf{2}\text{-}CO_2CO_2]^0$.

## Conclusions

In summary, the present work describes an unexplored mechanistic pathway for low-energy C-O bond cleavage in the reductive disproportionation of $CO_2$ to CO and $CO_3^{2-}$. Computational work in conjunction with IR and NMR spectroscopic detection of accumulated reaction intermediates established the involvement of an unprecedented 5-membered metallacyclic intermediate in the catalytic cycle. The formation of the metallacycle is enabled by the flexible ligation of the polypyridyl ligands, and it is shown that the ligand with the least binding strength

to the metal is the one that partially de-coordinates to liberate the coordination site required for metallacycle formation. The Ru center plays a dual role in the catalytic cycle: it acts as a Lewis base and attacks the first $CO_2$ molecule at an early stage of the cycle, while also acting as an intramolecular Lewis acidic site to stabilize the negative charge of the [**Ru**-$CO_2CO_2$]$^0$, thereby leading to the cyclic [**Ru**-$CO_2CO_2$]$^{0,c}$. The latter intermediate is crucial for energy-conserving turnover, as it allows for a third reduction at a more positive potential than that of the starting complexes **1**$^{2+}$ and **2**$^{2+}$. The thereby produced [**Ru**-$CO_2CO_2$]$^{-1,c}$ contains structural features that allow for relatively facile C-O bond cleavage with the calculated activation barrier for this step being dramatically decreased as compared to the 60 kcal mol$^{-1}$ required for C-O bond cleavage in the non-cyclic [**Ru**-$CO_2CO_2$]$^0$. Subsequent carbonate liberation and re-ligation of the polypyridine ligand closes the catalytic cycle, and gives the catalyst a good overall stability. The present report is the first of its kind that experimentally observes metallacyclic intermediates during catalytic turnover. Considering its simplicity, it may well be that similar species in other mononuclear catalysts have hitherto been overlooked. At the same time, its identification and operation offer a new design feature that can now be implemented consciously in future catalyst designs.

## Acknowledgements

The authors would like to acknowledge the Swedish National Infrastructure for Computing (SNIC), which is funded by the Swedish Research Council (VR) through grant agreement no. 2016-07213, in Linköping (NSC), for the computational resources. The computations were performed under project numbers SNIC2017/1-13, SNIC2018/3-1. SNIC2019/3-6 and SNIC2020/5-41. We acknowledge NordForsk foundation (No. 85378) for the Nordic University hub Nord$CO_2$. MA has been supported by the Swedish Research Council (VR) grant number 2018-05396, and the Knut & Alice Wallenberg (KAW) project CATSS (KAW 2016.0072). XC acknowledges the China Scholarship Council (CSC). HA and SO acknowledge the Swedish Energy Agency (grant number: 42029-1) for financial support.

## References

1. C. Costentin, S. Drouet, M. Robert and J.-M. Savéant, *J. Am. Chem. Soc.*, 2012, **134**, 11235-11242.
2. I. Azcarate, C. Costentin, M. Robert and J.-M. Savéant, *J. Am. Chem. Soc.*, 2016, **138**, 16639-16644.
3. C. Costentin, S. Drouet, M. Robert and J.-M. Savéant, *Science*, 2012, **338**, 90-94.
4. R. Francke, B. Schille and M. Roemelt, *Chem. Rev.*, 2018, **118**, 4631-4701.
5. F. Franco, M. F. Pinto, B. Royo and J. Lloret-Fillol, *Angew. Chem. Int. Ed.*, 2018, **57**, 4603-4606.
6. S. Fernández, F. Franco, C. Casadevall, V. Martin-Diaconescu, J. M. Luis and J. Lloret-Fillol, *J. Am. Chem. Soc.*, 2020, **142**, 120-133.
7. M. L. Clark, P. L. Cheung, M. Lessio, E. A. Carter and C. P. Kubiak, *ACS Catal.*, 2018, **8**, 2021-2029.
8. B. Merillas, E. Cuéllar, A. Diez-Varga, T. Torroba, G. García-Herbosa, S. Fernández, J. Lloret-Fillol, J. M. Martín-Alvarez, D. Miguel and F. Villafañe, *Inorg. Chem.*, 2020, **59**, 11152-11165.
9. P. Gerschel, A. L. Cordes, S. Bimmermann, D. Siegmund, N. Metzler-Nolte and U.-P. Apfel, *Z. Anorg. Allg. Chem.*, 2021, **647**, 968-977.
10. S. Sung, D. Kumar, M. Gil-Sepulcre and M. Nippe, *J. Am. Chem. Soc.*, 2017, **139**, 13993-13996.
11. M. Merrouch, M. Benvenuti, M. Lorenzi, C. Léger, V. Fourmond and S. Dementin, *JBIC Journal of Biological Inorganic Chemistry*, 2018, **23**, 613-620.
12. H. Dobbek, V. Svetlitchnyi, L. Gremer, R. Huber and O. Meyer, *Science*, 2001, **293**, 1281-1285.

13. M. Can, F. A. Armstrong and S. W. Ragsdale, *Chem. Rev.*, 2014, **114**, 4149-4174.
14. N. Elgrishi, M. B. Chambers, X. Wang and M. Fontecave, *Chem. Soc. Rev.*, 2017, **46**, 761-796.
15. S. Dey, T. K. Todorova, M. Fontecave and V. Mougel, *Angew. Chem. Int. Ed.*, 2020, **59**, 15726-15733.
16. M. E. Ahmed, A. Rana, R. Saha, S. Dey and A. Dey, *Inorg. Chem.*, 2020, **59**, 5292-5302.
17. E. Boutin, L. Merakeb, B. Ma, B. Boudy, M. Wang, J. Bonin, E. Anxolabéhère-Mallart and M. Robert, *Chem. Soc. Rev.*, 2020, **49**, 5772-5809.
18. T. Fogeron, T. K. Todorova, J.-P. Porcher, M. Gomez-Mingot, L.-M. Chamoreau, C. Mellot-Draznieks, Y. Li and M. Fontecave, *ACS Catal.*, 2018, **8**, 2030-2038.
19. T. Fogeron, P. Retailleau, M. Gomez-Mingot, Y. Li and M. Fontecave, *Organometallics*, 2019, **38**, 1344-1350.
20. A. Mouchfiq, T. K. Todorova, S. Dey, M. Fontecave and V. Mougel, *Chem. Sci.*, 2020, **11**, 5503-5510.
21. S. Gonell, J. Lloret-Fillol and A. J. M. Miller, *ACS Catal.*, 2021, **11**, 615-626.
22. S. Gonell, M. D. Massey, I. P. Moseley, C. K. Schauer, J. T. Muckerman and A. J. M. Miller, *J. Am. Chem. Soc.*, 2019, **141**, 6658-6671.
23. S. Gonell, E. A. Assaf, K. D. Duffee, C. K. Schauer and A. J. M. Miller, *J. Am. Chem. Soc.*, 2020, **142**, 8980-8999.
24. S. L. Hooe, J. M. Dressel, D. A. Dickie and C. W. Machan, *ACS Catal.*, 2020, **10**, 1146-1151.
25. S. L. Hooe, J. Moreno, A. Reid, E. Cook and C. Machan, *ChemRxiv Preprint*, 2021, **https://doi.org/10.26434/chemrxiv.14165951.v2**.
26. A. W. Nichols, S. Chatterjee, M. Sabat and C. W. Machan, *Inorg. Chem.*, 2018, **57**, 2111-2121.
27. J. J. Moreno, S. L. Hooe and C. W. Machan, *Inorg. Chem.*, 2021, **60**, 3635-3650.
28. R. Bonetto, R. Altieri, M. Tagliapietra, A. Barbon, M. Bonchio, M. Robert and A. Sartorel, *ChemSusChem*, 2020, **13**, 4111-4120.
29. L. Rotundo, C. Garino, E. Priola, D. Sassone, H. Rao, B. Ma, M. Robert, J. Fiedler, R. Gobetto and C. Nervi, *Organometallics*, 2019, **38**, 1351-1360.
30. C. Cometto, L. Chen, E. Anxolabéhère-Mallart, C. Fave, T.-C. Lau and M. Robert, *Organometallics*, 2019, **38**, 1280-1285.
31. C. Cometto, L. Chen, P.-K. Lo, Z. Guo, K.-C. Lau, E. Anxolabéhère-Mallart, C. Fave, T.-C. Lau and M. Robert, *ACS Catal.*, 2018, **8**, 3411-3417.
32. A. Maurin, C.-O. Ng, L. Chen, T.-C. Lau, M. Robert and C.-C. Ko, *Dalton Trans.*, 2016, **45**, 14524-14529.
33. L. Chen, Z. Guo, X.-G. Wei, C. Gallenkamp, J. Bonin, E. Anxolabéhère-Mallart, K.-C. Lau, T.-C. Lau and M. Robert, *J. Am. Chem. Soc.*, 2015, **137**, 10918-10921.
34. C. Costentin, M. Robert, J.-M. Savéant and A. Tatin, *Proc. Natl. Acad. Sci.*, 2015, **112**, 6882-6886.
35. C. Costentin, G. Passard, M. Robert and J.-M. Savéant, *J. Am. Chem. Soc.*, 2014, **136**, 11821-11829.
36. N. Queyriaux, K. Abel, J. Fize, J. Pécaut, M. Orio and L. Hammarström, *Sust. Energy & Fuels*, 2020, **4**, 3668-3676.
37. F. Franco, C. Cometto, L. Nencini, C. Barolo, F. Sordello, C. Minero, J. Fiedler, M. Robert, R. Gobetto and C. Nervi, *Chem. Eur. J.*, 2017, **23**, 4782-4793.
38. K. T. Ngo, M. McKinnon, B. Mahanti, R. Narayanan, D. C. Grills, M. Z. Ertem and J. Rochford, *J. Am. Chem. Soc.*, 2017, **139**, 2604-2618.
39. J. Agarwal, T. W. Shaw, H. F. Schaefer and A. B. Bocarsly, *Inorg. Chem.*, 2015, **54**, 5285-5294.
40. S. E. Tignor, T. W. Shaw and A. B. Bocarsly, *Dalton Trans.*, 2019, **48**, 12730-12737.
41. P. Gotico, L. Roupnel, R. Guillot, M. Sircoglou, W. Leibl, Z. Halime and A. Aukauloo, *Angew. Chem. Int. Ed.*, 2020, **59**, 22451-22455.
42. J. A. Buss, D. G. VanderVelde and T. Agapie, *J. Am. Chem. Soc.*, 2018, **140**, 10121-10125.
43. P. Sen, B. Mondal, D. Saha, A. Rana and A. Dey, *Dalton Trans.*, 2019, **48**, 5965-5977.
44. D. Z. Zee, M. Nippe, A. E. King, C. J. Chang and J. R. Long, *Inorg. Chem.*, 2020, **59**, 5206-5217.
45. M. Loipersberger, D. Z. Zee, J. A. Panetier, C. J. Chang, J. R. Long and M. Head-Gordon, *Inorg. Chem.*, 2020, **59**, 8146-8160.
46. M. H. Rønne, D. Cho, M. R. Madsen, J. B. Jakobsen, S. Eom, É. Escoudé, H. C. D. Hammershøj, D. U. Nielsen, S. U. Pedersen, M.-H. Baik, T. Skrydstrup and K. Daasbjerg, *J. Am. Chem. Soc.*, 2020, **142**, 4265-4275.

47. C. G. Margarit, C. Schnedermann, N. G. Asimow and D. G. Nocera, *Organometallics*, 2019, **38**, 1219-1223.
48. M. R. Madsen, J. B. Jakobsen, M. H. Rønne, H. Liang, H. C. D. Hammershøj, P. Nørby, S. U. Pedersen, T. Skrydstrup and K. Daasbjerg, *Organometallics*, 2020, **39**, 1480-1490.
49. S. Amanullah, P. Saha, A. Nayek, M. E. Ahmed and A. Dey, *Chem. Soc. Rev.*, 2021, **50**, 3755-3823.
50. S. Roy, B. Sharma, J. Pécaut, P. Simon, M. Fontecave, P. D. Tran, E. Derat and V. Artero, *J. Am. Chem. Soc.*, 2017, **139**, 3685-3696.
51. E. Haviv, D. Azaiza-Dabbah, R. Carmieli, L. Avram, J. M. L. Martin and R. Neumann, *J. Am. Chem. Soc.*, 2018, **140**, 12451-12456.
52. S. Sung, X. Li, L. M. Wolf, J. R. Meeder, N. S. Bhuvanesh, K. A. Grice, J. A. Panetier and M. Nippe, *J. Am. Chem. Soc.*, 2019, **141**, 6569-6582.
53. M. Hammouche, D. Lexa, M. Momenteau and J. M. Saveant, *J. Am. Chem. Soc.*, 1991, **113**, 8455-8466.
54. I. Bhugun, D. Lexa and J.-M. Savéant, *The Journal of Physical Chemistry*, 1996, **100**, 19981-19985.
55. M. D. Sampson and C. P. Kubiak, *J. Am. Chem. Soc.*, 2016, **138**, 1386-1393.
56. B. A. Johnson, S. Maji, H. Agarwala, T. A. White, E. Mijangos and S. Ott, *Angew Chem Int Ed Engl*, 2016, **55**, 1825-1829.
57. B. A. Johnson, H. Agarwala, T. A. White, E. Mijangos, S. Maji and S. Ott, *Chem. Eur. J.*, 2016, **22**, 14870-14880.
58. A. Gennaro, A. A. Isse and E. Vianello, *J. Electroanal. Chem. Interfacial Electrochem.*, 1990, **289**, 203-215.
59. Z. Chen, C. Chen, D. R. Weinberg, P. Kang, J. J. Concepcion, D. P. Harrison, M. S. Brookhart and T. J. Meyer, *Chem. Commun.*, 2011, **47**, 12607-12609.
60. J. Agarwal, E. Fujita, H. F. Schaefer and J. T. Muckerman, *J. Am. Chem. Soc.*, 2012, **134**, 5180-5186.
61. B. P. Sullivan, C. M. Bolinger, D. Conrad, W. J. Vining and T. J. Meyer, *J. Chem. Soc., Chem. Commun.*, 1985, DOI: 10.1039/C39850001414, 1414-1416.
62. C. W. Machan, S. A. Chabolla, J. Yin, M. K. Gilson, F. A. Tezcan and C. P. Kubiak, *J. Am. Chem. Soc.*, 2014, **136**, 14598-14607.
63. T. Herskovitz and L. J. Guggenberger, *J. Am. Chem. Soc.*, 1976, **98**, 1615-1616.
64. P. M. Jurd, H. L. Li, M. Bhadbhade and L. D. Field, *Organometallics*, 2020, **39**, 2011-2018.
65. M. Feller, U. Gellrich, A. Anaby, Y. Diskin-Posner and D. Milstein, *J. Am. Chem. Soc.*, 2016, **138**, 6445-6454.
66. J. Langer, W. Imhof, M. J. Fabra, P. García-Orduña, H. Görls, F. J. Lahoz, L. A. Oro and M. Westerhausen, *Organometallics*, 2010, **29**, 1642-1651.
67. R. Kempe, J. Sieler, D. Walther, J. Reinhold and K. Rommel, *Z. Anorg. Allg. Chem.*, 1993, **619**, 1105-1110.
68. L. Dahlenburg and C. Prengel, *J. Organomet. Chem.*, 1986, **308**, 63-71.
69. E. Carmona, F. Gonzalez, M. L. Poveda, J. M. Marin, J. L. Atwood and R. D. Rogers, *J. Am. Chem. Soc.*, 1983, **105**, 3365-3366.
70. F. Lucarini, J. Fize, A. Morozan, M. Marazzi, M. Natali, M. Pastore, V. Artero and A. Ruggi, *Sust. Energy & Fuels*, 2020, **4**, 589-599.
71. J. J. Leung, J. Warnan, K. H. Ly, N. Heidary, D. H. Nam, M. F. Kuehnel and E. Reisner, *Nature Catal.*, 2019, **2**, 354-365.
72. S. Aroua, T. K. Todorova, V. Mougel, P. Hommes, H.-U. Reissig and M. Fontecave, *ChemCatChem*, 2017, **9**, 2099-2105.
73. S. C. Cheng, C. A. Blaine, M. G. Hill and K. R. Mann, *Inorg. Chem.*, 1996, **35**, 7704-7708.
74. C. Jegat, M. Fouassier, M. Tranquille, J. Mascetti, I. Tommasi, M. Aresta, F. Ingold and A. Dedieu, *Inorg. Chem.*, 1993, **32**, 1279-1289.
75. The remaining calculated peaks at 1695 $cm^{-1}$ and 1291 $cm^{-1}$ for $[\mathbf{2}\text{-}CO_2CO_2]^{-1,c}$ are masked by the $CO_3^{2-}$ IR bands centered at 1686 $cm^{-1}$ and 1301 $cm^{-1}$ (Figures S6(d) and 6(b)).
76. Y. Arikawa, T. Nakamura, S. Ogushi, K. Eguchi and K. Umakoshi, *Dalton Trans.*, 2015, **44**, 5303-5305.